

Internal damping in rotating shafts

*Original*

Internal damping in rotating shafts / Vatta, Furio; Vigliani, Alessandro. - In: MECHANISM AND MACHINE THEORY. - ISSN 0094-114X. - 43:(2008), pp. 1376-1384. [10.1016/j.mechmachtheory.2007.12.009]

*Availability:*

This version is available at: 11583/1664475 since:

*Publisher:*

*Published*

DOI:10.1016/j.mechmachtheory.2007.12.009

*Terms of use:*

This article is made available under terms and conditions as specified in the corresponding bibliographic description in the repository

*Publisher copyright*

(Article begins on next page)

# Internal damping in rotating shafts

F. Vatta, A. Vigliani

Dipartimento di Meccanica - Politecnico di Torino  
C.so Duca degli Abruzzi, 24 - 10129 Torino - ITALY  
E-mail: [alessandro.vigliani@polito.it](mailto:alessandro.vigliani@polito.it)

**Keywords** internal damping, rotordynamics, nonlinear forces

**Abstract** *This paper analyses the influence of internal damping on the dynamic behaviour of rotating shafts. The problem is faced considering the presence of nonlinearities introduced in the restoring elastic forces by the alternate compression and extension of the shaft fibres; these forces show a component that can oppose or drive the shaft whirl motion.*

*The analytical solutions obtained allow to describe the transient motion of the shaft and to evaluate the stability limit, whose value slightly differs from the classical one determined with linear approaches.*

# 1 Introduction

The term “internal damping” is commonly adopted regarding both the elastic hysteresis of materials and the shaft fibre shear inside the hub (Yamamoto and Ishida, 2001; Tondl, 1965). When a rotating shaft undergoes a perturbation, consisting in displacement and velocity variations of a point belonging to the shaft axis with respect to dynamic equilibrium conditions, the fibres are alternatively compressed and stretched. This phenomenon occurs every time that the rotor angular speed  $\omega$  with respect to its deflected axis line differs from the whirl speed, i.e. the angular velocity  $\dot{\vartheta}$  of the deflection line itself.

The problem has been faced by many influential researchers; it is worth remembering, among others, Timoshenko (1947) and Den Hartog (1956) who proved the presence of a force normal to the plane of the deformed shaft, due to the fact that the neutral axis of strain does not coincide with the neutral line of stress.

The same result was obtained by Kimball (1924, 1925), who gave an explanation different from the previous ones, thus being able to analyse also the structural damping. Kimball’s experiments demonstrated the existence of an elastic restoring force that does not lie in the plane of the deflection curve, but is inclined of an angle  $2\mu$  with respect to the plane of bending; however, the most important result of his researches is the demonstration that the phase of the force is practically independent from the angular speed.

Hence, the analytical model commonly adopted to represent internal damping (i.e. Kelvin–Voigt model, see, e.g., Vatta and Vigliani (2003)), gives results that can be considered only partly adequate; in fact, this model predicts a force normal to the plane of the deflection line and proportional to the velocity of the shaft deflection in a system rotating with angular speed  $\omega$ , in contrast to the experimental evidence.

Recently, Dimentberg (2005) analysed the dynamic behaviour of a simple Jeffcott rotor in presence of a randomly varying rotating damping that may occasionally bring the rotor into the domain of dynamic instability.

In conclusion, if internal damping is modeled assuming that the restoring force is proportional to the deflected shaft velocity in the rotating system, then the equations describing the shaft perturbed motion are linear; moreover it is also well known that it is easy to compute the analytical solution.

However it is interesting to look for a solution of the problem more consistent with the experimental results. To this aim, it is necessary to drop the linear approach and to consider a deformed shaft rotating with angular speed  $\omega$  and whirling at velocity  $\dot{\vartheta}$ : it results that the elastic force is inclined of an angle  $2\mu$  that does not depend on the speed but only on the material.

When  $\omega > \dot{\vartheta}$  this restoring force shows a component tending to drive the shaft around in its path of whirl, whereas if  $\omega < \dot{\vartheta}$  an opposite situation occurs. Since for a given constant value of the angular velocity  $\omega$  the angular speed  $\dot{\vartheta}$  varies in time, both the previously described conditions can alternatively take place. Hence, even if the equations of motion are linear in the two different cases, the system itself is nonlinear, its response being not proportional to the excitation. This circumstance leads to a hereditary problem, whose solution determines the elastic deflections depending on the shaft angular speed and on the perturbed motion initial conditions; only under particular initial conditions the problem is linear.

In the present paper the authors study the dynamic behaviour of a rotating shaft through a nonlinear approach. The results are similar to those already known, obtained with a linear approach. However, it is worth underlining that the approach used in the present work allows to highlight the shaft behaviour just during the transitory that leads, depending on the initial conditions, to stability or instability; such behaviour is completely ignored when an asymptotic stability methodology is applied.

# 2 Analysis

Consider an elastic shaft with a disk having mass  $m$ , statically and dynamically balanced, driven by a motor rotating at constant angular speed. In the deflected configuration the elastic force is directed as in Fig. 1 if  $\omega > \dot{\vartheta}$ , whereas it is symmetric to  $OG$  if  $\omega < \dot{\vartheta}$ .

The equilibrium equations for the rotor are:

$$m\ddot{x} + k \left[ x \cos(2\mu) + y \sin(2\mu) \right] = 0 \quad (1)$$

$$m\ddot{y} - k \left[ x \sin(2\mu) - y \cos(2\mu) \right] = 0, \quad (2)$$

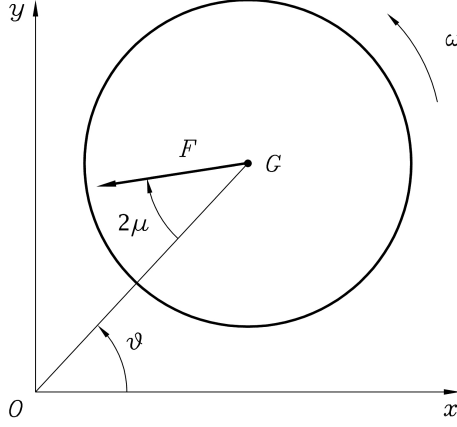


Figure 1: Section of the shaft

where  $k$  is the shaft stiffness and  $x$  and  $y$  are the coordinates of the centre of mass  $G$ . Let  $z = x + iy$ ; then it holds

$$m\ddot{z} + kz [\cos(2\mu) - i \sin(2\mu)] = 0. \quad (3)$$

Since for regular steel  $\mu$  is small ( $\mu \approx 10^{-3}$  rad), then Eq. (3) can be split into

$$m\ddot{z} + kz(1 - i2\mu) = 0 \quad \text{if} \quad \omega > \dot{\vartheta} \quad (4)$$

$$m\ddot{z} + kz(1 + i2\mu) = 0 \quad \text{if} \quad \omega < \dot{\vartheta}, \quad (5)$$

whose solution is given by:

$$z = A_0 e^{ipt} + B_0 e^{-ipt}, \quad (6)$$

where

$$p = \sqrt{\frac{k}{m} \sqrt{1 + 4\mu^2}} e^{\mp \frac{1}{2} i \tan^{-1}(2\mu)}. \quad (7)$$

Let

$$\omega_0 = \sqrt{\frac{k}{m} \sqrt{1 + 4\mu^2}}; \quad (8)$$

then, since

$$\frac{1}{2} i \tan^{-1}(2\mu) \approx i\mu \quad \text{and} \quad e^{\pm i\mu} \approx 1 \pm i\mu, \quad (9)$$

Eq. (6) becomes:

$$z = A(t) e^{i\omega_0 t} + B(t) e^{-i\omega_0 t} \quad (10)$$

with

$$A(t) = A_0 e^{\mu\omega_0 t} \quad \text{and} \quad B(t) = B_0 e^{-\mu\omega_0 t} \quad \text{for} \quad \omega > \dot{\vartheta} \quad (11)$$

$$A(t) = A_0 e^{-\mu\omega_0 t} \quad \text{and} \quad B(t) = B_0 e^{\mu\omega_0 t} \quad \text{for} \quad \omega < \dot{\vartheta}. \quad (12)$$

Hence the elastic deflection can be expressed as the sum of two counter-rotating vectors with angular speed  $\omega_0$ ; at a given time  $t$ , the amplitudes  $A(t)$  and  $B(t)$  show opposite behaviour, i.e. one grows while the other one decreases. The constants  $A_0$  and  $B_0$  depend on the initial position and velocity of the centre of mass  $G$ ; if time is measured starting from the instant at which the two

counter-rotating vectors superimpose on the  $x$  axis, such constants are real and positive. Since the sum of the two counter-rotating vectors can be expressed as a single vector, it holds:

$$A(t) e^{i\omega_0 t} + B(t) e^{-i\omega_0 t} = C(t) e^{i\vartheta(t)}, \quad (13)$$

where

$$\tan \vartheta = \frac{A(t) - B(t)}{A(t) + B(t)} \tan(\omega_0 t). \quad (14)$$

The angular speed  $\dot{\vartheta}$  of vector  $\vec{C}$ , i.e. the whirl velocity, can be obtained from Eq. (14):

$$\dot{\vartheta} = \frac{\lambda^2 - 1}{\lambda^2 + 2\lambda \cos(2\omega_0 t) + 1} \omega_0, \quad (15)$$

where  $\lambda = A(t)/B(t)$ ; this result is drawn under the hypothesis of  $\lambda$  varying very slowly in time, i.e. considering  $\lambda$  constant in the period  $T = 2\pi/\omega_0$ .

Equation (15) highlights the fact that the whirl speed  $\dot{\vartheta}$  fluctuates between a minimum and a maximum; it yields:

$$\frac{\lambda - 1}{\lambda + 1} \leq \frac{\dot{\vartheta}}{\omega_0} \leq \frac{\lambda + 1}{\lambda - 1} \quad \text{if } \lambda > 1 \quad (16)$$

$$\frac{\lambda + 1}{\lambda - 1} \leq \frac{\dot{\vartheta}}{\omega_0} \leq \frac{\lambda - 1}{\lambda + 1} \quad \text{if } \lambda < 1. \quad (17)$$

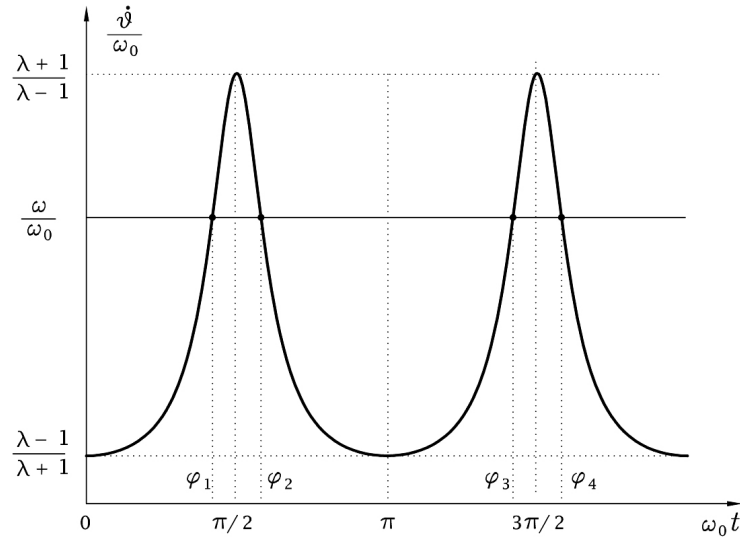


Figure 2: Whirl speed fluctuations with respect to time ( $\lambda = 2$ )

Figure 2 shows the whirl velocity versus  $\omega_0 t$  for a given value of  $\lambda$  greater than 1, while Fig. 3 shows the diagrams of  $(\dot{\vartheta}/\omega_0)_{\min}$  and  $(\dot{\vartheta}/\omega_0)_{\max}$  versus  $\lambda$ . In this figure, four regions can be identified:

region I:	$0 \leq \lambda \leq 1$	$\omega/\omega_0 \geq 0$
region II:	$\lambda > 1$	$\omega/\omega_0 > (\dot{\vartheta}/\omega_0)_{\max}$
region III:	$\lambda > 1$	$0 \leq \omega/\omega_0 < (\dot{\vartheta}/\omega_0)_{\min}$
region IV:	$\lambda > 1$	$(\dot{\vartheta}/\omega_0)_{\min} \leq \omega/\omega_0 \leq (\dot{\vartheta}/\omega_0)_{\max}$

It is possible to consider only the values of  $\omega > 0$  without loss of generality; hence, in the following analysis, the authors will study the behaviour of the shaft for given initial conditions of the perturbed motion (represented by a point  $P_0(\omega, \lambda_0)$  in the plane of Fig. 3). If  $P_0$  lies in region II, then  $\omega > \dot{\vartheta}$  and hence Eq.(11) holds, so that  $A(t)$  grows with time, whereas  $B(t)$  decreases;

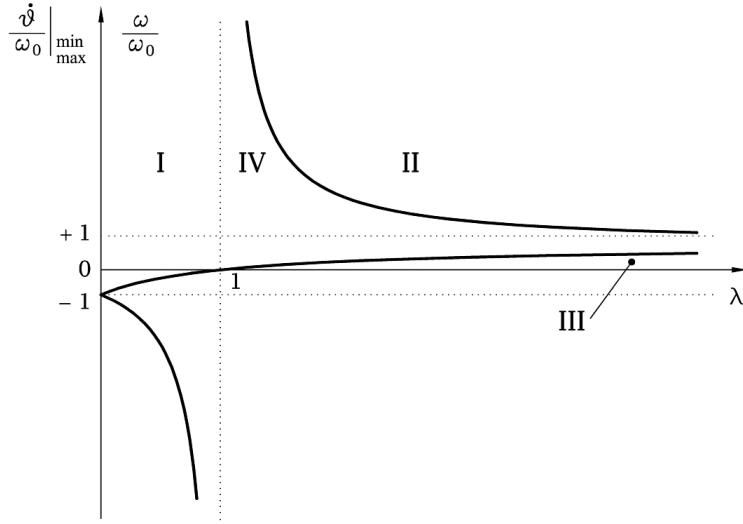


Figure 3: Maximum and minimum values of whirl speed  $\dot{\vartheta}/\omega_0$

consequently  $\lambda$  increases unlimitedly. The system status is characterized by a point  $P(t)$  moving along a line through  $P_0$  parallel to the  $x$  axis: hence the solution diverges and consequently the shaft is unstable. Such case corresponds to the linear behaviour.

If point  $P_0$  belongs to region I, where  $\omega > \dot{\vartheta}$ , again  $\lambda$  grows with time and hence  $P(t)$  moves along a parallel to the  $x$  axis entering region IV; if  $P_0$  lies in region III, where  $\omega < \dot{\vartheta}$ , it holds Eq. (12) and then  $A(t)$  decreases while  $B(t)$  grows, with a consequent decrease of  $\lambda$  that leads point  $P$  into region IV. Hence, it is necessary to investigate the shaft behaviour inside region IV, where angular speed  $\omega$  is alternatively greater or smaller than  $\dot{\vartheta}$ . In the time  $T$  correspondent to the angle  $2\pi$  ( $T = 2\pi/\omega_0$ ), with the assumption of negligible variations of  $\lambda$ , there occur four changes of sign of the difference  $\omega - \dot{\vartheta}$  in correspondence of angles  $\varphi_1, \varphi_2, \varphi_3$  and  $\varphi_4$  (see Fig. 2). Equations (11) and (12) hold in turn for successive time intervals; obviously the constants must be computed imposing the continuity of position and velocity at each interval limits and hence the problem has hereditary characteristics. The motion is a continuous sequence of cycles analogous to those represented in Fig. 2; hence the set of sign variations is given by:

$$\begin{aligned} 0 \div 2\pi & \rightarrow \varphi_1, \varphi_2, \varphi_3, \varphi_4 \\ \pi \div \pi + 2\pi & \rightarrow \varphi_3, \varphi_4, \varphi_5, \varphi_6 \\ 2\pi \div 2\pi + 2\pi & \rightarrow \varphi_5, \varphi_6, \varphi_7, \varphi_8 \end{aligned}$$

and, in general, it yields:

$$n\pi \div n\pi + 2\pi \rightarrow \varphi_{2n+1}, \varphi_{2n+2}, \varphi_{2n+3}, \varphi_{2n+4} \quad (18)$$

with  $n = 0, 1, 2, \dots$

Moreover it holds:

$$\begin{aligned} \varphi_{2n+1} + \varphi_{2n+2} &= (2n+1)\pi \\ \varphi_{2n+3} - \varphi_{2n+1} &= \pi \\ \varphi_{2n+4} - \varphi_{2n+2} &= \pi; \end{aligned}$$

furthermore, in the intervals  $\varphi_{2n} < \varphi < \varphi_{2n+1}$  and  $\varphi_{2n+2} < \varphi < \varphi_{2n+3}$ , Eq. (11) holds, while in the intervals  $\varphi_{2n+1} < \varphi < \varphi_{2n+2}$  and  $\varphi_{2n+3} < \varphi < \varphi_{2n+4}$ , Eq. (12) holds [ $\varphi_0 = 0$ ].

The expression of deflection  $z$  after the  $n^{th}$  sign variation of  $\omega - \dot{\vartheta}$  can be obtained equating the final conditions at the limits of each time interval where the form of the equation doesn't change, with the initial conditions of the following interval. Thus, if  $\varphi_1 = \omega_0 t_1$  is the angle correspondent to the first sign variation of  $\omega - \dot{\vartheta}$ , it yields:

$$\begin{aligned} A_0 e^{\mu\varphi_1 + \imath\varphi_1} + B_0 e^{-\mu\varphi_1 - \imath\varphi_1} &= A_1 + B_1 \\ (\imath + \mu)(A_0 e^{\mu\varphi_1 + \imath\varphi_1} - B_0 e^{-\mu\varphi_1 - \imath\varphi_1}) &= (\imath - \mu)(A_1 - B_1) \end{aligned} \quad (19)$$

that leads to

$$\begin{aligned}
2A_1 &= e^{\mu\varphi_1} e^{\imath\varphi_1} \left[ A_0 + B_0 e^{-2\mu\varphi_1} e^{-2\imath\varphi_1} + \right. \\
&\quad \left. + \frac{\imath + \mu}{\imath - \mu} (A_0 - B_0 e^{-2\mu\varphi_1} e^{-2\imath\varphi_1}) \right] \\
2B_1 &= e^{\mu\varphi_1} e^{\imath\varphi_1} \left[ A_0 + B_0 e^{-2\mu\varphi_1} e^{-2\imath\varphi_1} + \right. \\
&\quad \left. - \frac{\imath + \mu}{\imath - \mu} (A_0 - B_0 e^{-2\mu\varphi_1} e^{-2\imath\varphi_1}) \right].
\end{aligned} \tag{20}$$

Since  $\mu A_0 \ll A_0$  and  $\mu B_0 \ll B_0$ , then, neglecting the terms of order  $\mu^2$ , it holds:

$$A_1 = e^{\imath\varphi_1} \left[ A_0 (1 + \mu\varphi_1) + \imath\mu B_0 e^{-2\imath\varphi_1} \right] \tag{21}$$

$$B_1 = e^{-\imath\varphi_1} \left[ B_0 (1 - \mu\varphi_1) + \imath\mu A_0 e^{2\imath\varphi_1} \right]. \tag{22}$$

Similarly it yields:

$$\begin{aligned}
A_2 &= e^{\imath\varphi_2} \left\{ A_0 \left[ 1 + \mu\varphi_1 - \mu(\varphi_2 - \varphi_1) \right] + \right. \\
&\quad \left. + \imath\mu B_0 \left[ e^{-2\imath\varphi_1} - e^{-2\imath\varphi_2} \right] \right\} \\
B_2 &= e^{-\imath\varphi_2} \left\{ B_0 \left[ 1 - \mu\varphi_1 + \mu(\varphi_2 - \varphi_1) \right] + \right. \\
&\quad \left. + \imath\mu A_0 \left[ e^{2\imath\varphi_1} - e^{2\imath\varphi_2} \right] \right\},
\end{aligned} \tag{23}$$

and, in general,

$$\begin{aligned}
A_n &= e^{\imath\varphi_n} \left\{ A_0 \left[ 1 + \mu\varphi_1 - \mu(\varphi_2 - \varphi_1) + \mu(\varphi_3 - \varphi_2) - \mu(\varphi_4 - \varphi_3) + \dots \right] + \right. \\
&\quad \left. + \imath\mu B_0 \left[ e^{-2\imath\varphi_1} - e^{-2\imath\varphi_2} + e^{-2\imath\varphi_3} - e^{-2\imath\varphi_4} + \dots \right] \right\} \\
B_n &= e^{-\imath\varphi_n} \left\{ B_0 \left[ 1 - \mu\varphi_1 + \mu(\varphi_2 - \varphi_1) - \mu(\varphi_3 - \varphi_2) + \mu(\varphi_4 - \varphi_3) + \dots \right] + \right. \\
&\quad \left. + \imath\mu A_0 \left[ e^{2\imath\varphi_1} - e^{2\imath\varphi_2} + e^{2\imath\varphi_3} - e^{2\imath\varphi_4} + \dots \right] \right\}.
\end{aligned} \tag{24}$$

Therefore, deflection  $z$  after the  $n^{th}$  sign variation is given by

$$z_n = \tilde{A}_n e^{\imath\varphi_n} + \tilde{B}_n e^{-\imath\varphi_n}, \tag{25}$$

where  $\tilde{A}$  and  $\tilde{B}$  are given by the expressions between braces in Eq. (24).

Consider now the time interval defined by  $\varphi_1$  and  $\varphi_3$ , corresponding to a complete oscillation of the whirl speed; it holds

$$\begin{aligned}
\tilde{A}_1 &= A_0 + \mu A_0 \varphi_1 + \imath\mu B_0 e^{-2\imath\varphi_1} \\
\tilde{A}_3 &= A_0 + \mu A_0 \varphi_1 - \mu A_0 (\varphi_2 - \varphi_1) + \mu A_0 (\varphi_3 - \varphi_2) + \\
&\quad + \imath\mu B_0 (e^{-2\imath\varphi_1} - e^{-2\imath\varphi_2} + e^{-2\imath\varphi_3}),
\end{aligned} \tag{26}$$

and hence:

$$\begin{aligned}
\tilde{A}_3 &= \tilde{A}_1 + \mu A_0 \left[ (\varphi_1 - \varphi_2) - (\varphi_2 - \varphi_3) \right] + \\
&\quad + \imath\mu B_0 (-e^{-2\imath\varphi_2} + e^{-2\imath\varphi_3}).
\end{aligned} \tag{27}$$

Similarly:

$$\begin{aligned}
\tilde{B}_3 &= \tilde{B}_1 - \mu B_0 \left[ (\varphi_1 - \varphi_2) - (\varphi_2 - \varphi_3) \right] + \\
&\quad + \imath\mu A_0 (-e^{2\imath\varphi_2} + e^{2\imath\varphi_3}).
\end{aligned} \tag{28}$$

These expressions hold for the general time interval correspondent to a complete oscillation of the whirl speed, hence also for the interval  $\varphi_{2n+1} \div \varphi_{2n+3}$ ,  $n \neq 0$ . It results:

$$\begin{aligned}\tilde{A}_{2n+3} &= \tilde{A}_{2n+1} + \mu A_0 \left[ (\varphi_{2n+1} - \varphi_{2n+2}) - (\varphi_{2n+2} - \varphi_{2n+3}) \right] \\ &+ i\mu B_0 \left( -e^{-2i\varphi_{2n+2}} + e^{-2i\varphi_{2n+3}} \right) \\ \tilde{B}_{2n+3} &= \tilde{B}_{2n+1} - \mu B_0 \left[ (\varphi_{2n+1} - \varphi_{2n+2}) - (\varphi_{2n+2} - \varphi_{2n+3}) \right] \\ &+ i\mu A_0 \left( -e^{2i\varphi_{2n+2}} + e^{2i\varphi_{2n+3}} \right).\end{aligned}\tag{29}$$

Moreover it holds:

$$\varphi_{2n+1} - \varphi_{2n+2} = 2\varphi_{2n+1} - (2n+1)\pi\tag{30}$$

$$\varphi_{2n+2} - \varphi_{2n+3} = -2\varphi_{2n+1} + 2n\pi\tag{31}$$

and

$$\cos(2\varphi_{2n+2}) = \cos(2\varphi_{2n+3})\tag{32}$$

$$\sin(2\varphi_{2n+2}) = -\sin(2\varphi_{2n+3});\tag{33}$$

hence:

$$\begin{aligned}\tilde{A}_{2n+3} &= \tilde{A}_{2n+1} + \mu A_0 [4(\varphi_{2n+1} - n\pi) - \pi] + \\ &+ 2\mu B_0 \sin(2\varphi_{2n+1}) \\ \tilde{B}_{2n+3} &= \tilde{B}_{2n+1} - \mu B_0 [4(\varphi_{2n+1} - n\pi) - \pi] + \\ &- 2\mu A_0 \sin(2\varphi_{2n+1}).\end{aligned}\tag{34}$$

Let  $\Phi = \varphi_{2n+1} - n\pi$ , then Eq. (34) becomes:

$$\begin{aligned}\tilde{A}_{2n+3} &= \tilde{A}_{2n+1} + \mu A_0 (4\Phi - \pi) + 2\mu B_0 \sin(2\Phi) = \\ &= \tilde{A}_{2n+1} + \mu (A_0 F_1 + B_0 F_2) \\ \tilde{B}_{2n+3} &= \tilde{B}_{2n+1} - \mu B_0 (4\Phi - \pi) - 2\mu A_0 \sin(2\Phi) \\ &= \tilde{B}_{2n+1} - \mu (B_0 F_1 + A_0 F_2)\end{aligned}\tag{35}$$

where, obviously,  $F_1 = 4\Phi - \pi$  and  $F_2 = 2\sin(2\Phi)$ .

### 3 Stability

Equations (35) give the values of amplitudes  $A$  and  $B$  after a complete oscillation and represent the starting conditions of the following cycle. Therefore it is possible to analyse the shaft stability highlighting the time history of amplitudes  $A$  and  $B$ . The first step is to evaluate the value  $\bar{\lambda}$ , real and positive, given by the ratio  $A/B$  at the time correspondent to  $\varphi_{2n+1}$ : it can be obtained from Eq. (15) by substituting  $\dot{\vartheta}$  and  $\omega_0 t$  respectively by  $\omega$  and  $\Phi$ . Let  $\nu = \omega_0/\omega$ ; then it yields:

$$\bar{\lambda} = \frac{-\cos(2\Phi) \pm \sqrt{\cos^2(2\Phi) - (1 - \nu^2)}}{1 - \nu}.\tag{36}$$

It is worth noting that in the case  $\nu > 1$ , since  $\bar{\lambda}$  must be real and positive, it holds:

$$\bar{\lambda} = \frac{\cos(2\Phi) + \sqrt{\nu^2 - \sin^2(2\Phi)}}{\nu - 1}\tag{37}$$



with  $0 \leq \Phi \leq \pi/2$ , as shown in Fig. 2. If  $\nu < 1$ , there are two solutions  $\bar{\lambda}$  for any value of  $\Phi$  belonging to the interval  $[\pi/4, \pi/2]$ :

$$\bar{\lambda} = \frac{\cos(2\Phi) \pm \sqrt{\nu^2 - \sin^2(2\Phi)}}{\nu - 1}. \quad (38)$$

It is now possible to examine the behaviour of the shaft inside region IV of Fig. 3. The cases of  $\omega$  greater or smaller than  $\omega_0$  will be analysed separately.

### 3.1 Case $\omega < \omega_0$ ( $\nu > 1$ )

Figure 4 plots  $\bar{\lambda}$  versus  $\Phi$  for different values of  $\nu$ , showing that  $\bar{\lambda}$  decreases with  $\Phi$ .

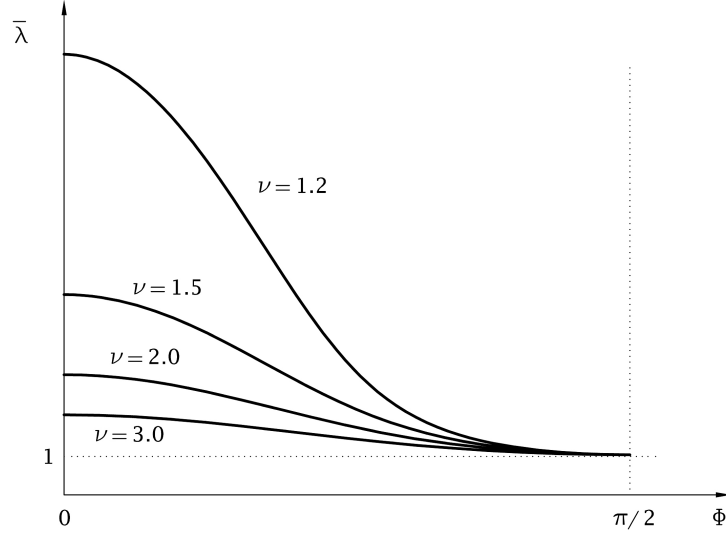


Figure 4: Solution  $\bar{\lambda}$  versus  $\Phi$  when  $\nu > 1$

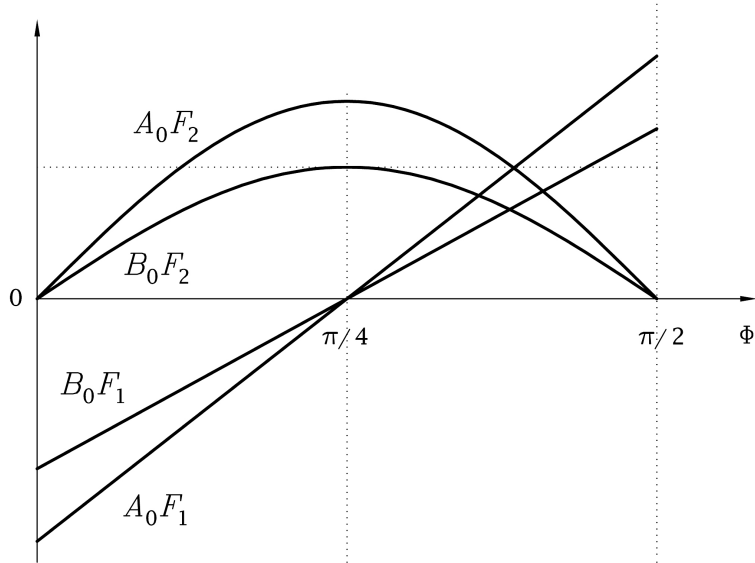


Figure 5: Functions  $F_1$  and  $F_2$  versus  $\Phi$

Since the initial conditions is characterized by  $\bar{\lambda} \geq 1$ , then  $A_0 > B_0$ . Figure 5 is a qualitative plot of functions  $A_0 F_1$ ,  $B_0 F_1$ ,  $A_0 F_2$  and  $B_0 F_2$ , while functions  $A_0 F_1 + B_0 F_2$  and  $A_0 F_2 + B_0 F_1$  are

shown in Fig. 6. The last functions cross the  $\Phi$  axis in  $H$  and  $K$ ; hence it is possible to identify three intervals:

- (a)  $0 < \Phi < \Phi_H$ , where  $A$  decreases while  $B$  grows: hence  $\bar{\lambda}$  decreases;
- (b)  $\Phi_H < \Phi < \Phi_K$ , where both  $A$  and  $B$  decrease;
- (c)  $\Phi_K < \Phi < \pi/2$ , where  $A$  grows while  $B$  decreases and hence  $\bar{\lambda}$  grows.

Therefore, if the initial conditions are such that  $\Phi$  lies in the first (a) or in the third (c) interval,  $\Phi$  grows or decreases respectively (see Fig. 4), up to the second (b) interval limits, where  $A$  and  $B$  decrease at the same time until vanishing; hence the case under analysis is stable. In fact, if  $\Phi$  is initially in the first or second interval, then the amplitudes are always reducing, while if it belongs to the third interval (c), amplitudes initially grow and then decrease until they vanish.

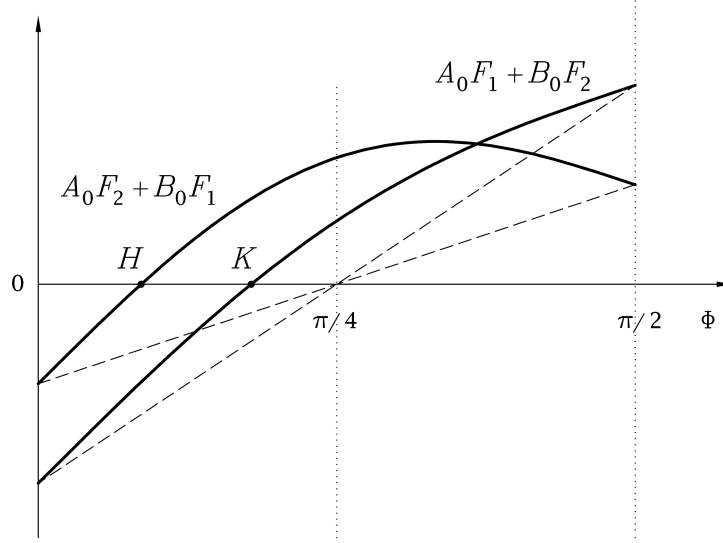


Figure 6: Functions  $A_0 F_1 + B_0 F_2$  and  $A_0 F_2 + B_0 F_1$  versus  $\Phi$

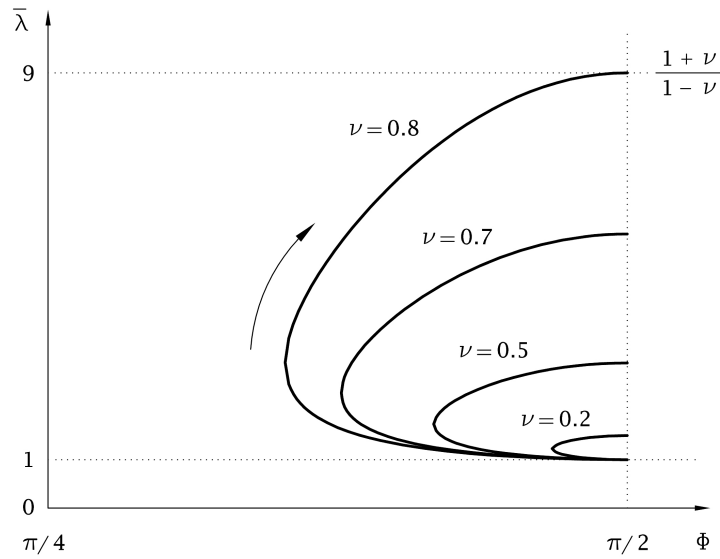


Figure 7: Solutions  $\bar{\lambda}$  versus  $\Phi$  with  $\nu < 1$

### 3.2 Case $\omega > \omega_0$ ( $\nu < 1$ )

Figure 7 plots  $\bar{\lambda}$  versus  $\Phi$  for different values of  $\nu$ ; as previously observed, for  $\pi/4 < \Phi < \pi/2$  the solution  $\bar{\lambda}$  are real and positive. From Fig. 6 it results that  $A$  grows while  $B$  decreases, so that  $\bar{\lambda}$  increases with time; hence curves in Fig. 7 are covered clockwise. Therefore the solutions reach value  $\pi/2$  and then enter region II (see Fig. 3), where  $\bar{\lambda}$  continuously grows, causing the shaft instability.

## 4 Conclusions

The influence of internal (hysteretic or structural) damping on rotating shafts stability represents a problem that has been studied since 1924. The most important result of the researches lies in the fact that the shaft appears to be unstable for angular speeds greater than the critical velocity, whereas its motion is stable for smaller speeds. However this result is usually obtained through a linear model of the internal damping that, on the contrary, has nonlinear characteristics.

In this paper the authors' approach to the problem considers a model that is more adequate to represent experimental evidence (Yamamoto and Ishida, 2001): as a matter of fact, the elastic force is assumed to be inclined with respect to the deflection plane of an angle that does depend on the angular speed. It is shown that only for particular initial conditions the problem can be regarded to as linear, as it happens in region II of Fig. 3; in general the problem is hereditary. The stability analysis is faced by studying how elastic deflection varies with time. The fluctuations of the whirl speed provoke alternate changes of the elastic force angle that correspond to a change of the motion differential equations, whose validity is limited to a certain time interval, i.e. until a successive phase variation occurs. It is worth noting that the analysis here presented allows to describe the shaft transient motion in case of both supercritical and subcritical speeds.

Finally, the nonlinear approach followed in the present study permits to highlight the following result: the value  $\omega_0$  of the angular speed that represent the stability threshold (i.e. the critical speed) differs from the value that can be computed adopting a linear model. This difference represent an interesting result from a qualitative point of view, even if it can be quantitatively negligible. In fact, the stability limit obtained with a linear approach (see, e.g., (Tondl, 1965)) is

$$\omega_0^2 = \frac{k}{m} - \left( \frac{h}{2m} \right)^2, \quad (39)$$

where  $k$ ,  $m$  and  $h$  are respectively the shaft stiffness, the disk mass and the internal friction coefficient. Conversely, as stated in Eq. (8), the nonlinear model leads to the value:

$$\omega_0^2 = \frac{k}{m} \sqrt{1 + 4\mu^2}, \quad (40)$$

where  $2\mu$  is the phase angle of the elastic force. Consequently, the different effect of internal damping on the critical speed as demonstrated above is made evident by using the methodology developed in the present contribution.

## References

- Den Hartog, P., 1956. Mechanical vibrations, Mc Graw-Hill, New York.
- Dimentberg, M. F., 2005. Vibration of a rotating shaft with randomly varying internal damping, J. of Sound and Vibration, 285, 759–765
- Kimball, A. L., 1924. Internal friction theory of shaft whirling, General Electric Rev. 27, 224–251.
- Kimball, A. L., 1924. Measurement of internal friction in a revolving deflected shaft, General Electric Rev. 28, 554–558.
- Timoshenko, S., 1947. Théorie des vibrations, Beranger, Paris.
- Tondl, A., 1965. Some problems of rotor dynamics, Chapman et Hall, London.
- Vatta, F., Vigliani, A., 2003. Il rotore di Jeffcott, Clut, Torino.
- Yamamoto, T., Ishida, S., 2001. Linear and nonlinear rotordynamics, John Wiley, New York.